The Kinetics and Phase Patterns in a Ternary Mixture Coupled with Chemical Reaction of A + B C

ARTICLE *in* THE JOURNAL OF PHYSICAL CHEMISTRY B · SEPTEMBER 2001

Impact Factor: 3.3 · DOI: 10.1021/jp011536p

3 AUTHORS, INCLUDING:

Bo Liu
Leibniz Institute for Baltic Sea Research
18 PUBLICATIONS **178** CITATIONS
SEE PROFILE

Chaohui Tong
Ningbo University
25 PUBLICATIONS **156** CITATIONS
SEE PROFILE

The Kinetics and Phase Patterns in a Ternary Mixture Coupled with Chemical Reaction of $A + B \underset{\Gamma_{-1}}{\overset{\Gamma_1}{\rightleftarrows}} C$

Bo Liu, Chaohui Tong, and Yuliang Yang*

Department of Macromolecular Science, Key Lab of Molecular Engineering of Polymers, SMEC, Fudan University, Shanghai, 200433, China

Received: April 23, 2001; In Final Form: July 31, 2001

In this paper, the phase separation of A, B, and C ternary mixtures coupled with the chemical reaction of $A + B \underset{\Gamma_{-1}}{\overset{\Gamma_1}{\rightleftarrows}} C$ is investigated numerically on the basis of the modified time-dependent Ginzburg−Landau (TDGL) equation. The simulation results showed that, depending on the rate constant of chemical reaction and the compatibility between the components, very complicated phase patterns could be obtained. It is found that when the compatibility of A and B is poor and C has good compatibility with A/B, in the early stage of phase evolution, the phase separation between A and B pushes C to the interface between A- and B-rich domains. However, when A and B are compatible while C and A/B are incompatible, in the early stage of phase evolution, C-rich spherical droplets are immersed in the A/B continuous phase. As evolution goes on, the phase separation of A and B takes place and pushes C droplets to the interface between A- and B-rich domains. It is also found that the phase evolution depends on the competition between chemical reaction and phase separation. In the case of a relatively large reaction rate constant, the effect of chemical reaction is dominant, the phase separation between C and A/B is inhibited, and the phase separation between A and B takes place. As the phase separation of A and B proceeds, C decomposes into A and B rapidly, resulting in the phase pattern of small amount of C distributed along the interface between A- and B-rich domains. As the reaction rate constant gradually decreases, the effect of chemical reaction is diminishing. In the late stage of phase separation, the concentration of C increases as the rate constant of chemical reaction decreases, and the C-rich phase changes from dispersed droplets to the continuous thin phase. Therefore, the phase separation between A and B can only be confined in small regions, resembling the case of binary mixture of A and B homopolymers with AB diblock copolymers. The above results reveal importantly that due to the phase separation between the components A, B, and C, the global equilibrium, which exists in the homogeneous mixture, does not exist in the phase separating system. The overall volume fraction of C could be either lower or higher than the equilibrium value for the homogeneous mixture, depending on the compatibility between the components and the rate constant of coupled chemical reaction.

I. Introduction

Reaction−diffusion systems are ubiquitous in nature. Many reaction−diffusion systems can generate fascinating spatial−temporal patterns, such as spiral waves, etc.[1] Among them, the Belousov−Zhabotinsky reaction[2] is probably the most extensively studied reaction−diffusion system, and the autocatalytic reactions in biological systems[3,4] also attract much attention. Directed by symmetry breaking, small molecules and polymer blends can form various phase diagrams through spinodal decomposition and, later, growth.[5,6] One can undoubtedly expect that, when coupled with phase separation, the reaction−diffusion systems could generate even more complex spatial−temporal patterns. Through experimental studies, people have observed the pattern formation and selection in the systems of phase separation coupled with chemical reaction, such as epoxy-toughened rubber,[7] photochemically cross-linking reactions,[8,9] etc. Glotzer[10,11] et al. studied the phase separation dynamics of binary mixture coupled with the simple chemical reaction of type $A \underset{\Gamma_{-1}}{\overset{\Gamma_1}{\rightleftarrows}} B$ by numerical simulation based on the time-dependent Ginzburg−Landau (TDGL) equation coupled with this simple chemical reaction. They found that the size of the ordered phase domains is confined in a certain length scale by the chemical reaction.

However, the phase separation coupled chemical reactions investigated in the literature are much too simple. In this paper, we studied a ternary blends system, where a reversible chemical reaction exist

$$A + B \underset{\Gamma_{-1}}{\overset{\Gamma_1}{\rightleftharpoons}} C \qquad (1)$$

Γ_1 and Γ_{-1} in the above equation represent the temperature-dependent forward and backward reaction rate constants,

* To whom the correspondence should be addressed.

10.1021/jp011536p CCC: $20.00
Published on Web 09/26/2001

respectively. When the system at equilibrium is quenched to an unstable phase region, the change in reaction rate constants will shift the reaction either backward or forward, and species A, B, and C will then reestablish at a new equilibrium. On the other hand, due to the decrease of pair interaction between A, B, and C, phase separation among A, B, and C will take place. These two processes are competing with each other and affect the phase pattern selection and evolution.[12,13,14] It should be mentioned that this system is more complex than the system studied by Glotzer[10,11] et al.

In this paper, we carry out computer simulations in two dimensions to study the kinetics and morphology for the ternary mixture coupled with the above chemical reaction based on the modified TDGL equation and using the cell dynamical scheme (CDS).[15,16] The paper is organized as follows. In section II, the free energy functional for a ternary mixture and the modified TDGL equation for the numerical simulation are given. In section III, we discuss the competition between phase separation and reversible chemical reaction and its effects on the kinetics and morphologies of the model system. The discussion will consider the compatibility between the species A, B, and C. Section IV gives the conclusions drawn in this work.

II. Model Equations and Simulation Algorithm

The Flory−Huggins free energy for the ternary mixture can be written as[17,18]

$$f(\varphi_A,\varphi_B,\varphi_C) = \frac{1}{N_A}\varphi_A \ln(\varphi_A) + \frac{1}{N_B}\varphi_B \ln(\varphi_B) + \frac{1}{N_C}\varphi_C \ln(\varphi_C) + \chi_{AB}\varphi_A\varphi_B + \chi_{AC}\varphi_A\varphi_C + \chi_{BC}\varphi_B\varphi_C \quad (2)$$

where φ_A, φ_B, and φ_C are the volume fractions of species A, B, and C, respectively. N_A, N_B, and N_C are the chain lengths of A, B, and C, respectively. χ_{ij} is the interaction parameter between the segments i and j, and i, j = A, B, and C. In this ternary mixture, under the incompressible condition, only two of the local volume fractions are independent. Following the method proposed by Ohta and Ito,[19,20] two order parameters, η and ϕ, are defined as

$$\phi = \varphi_A - \varphi_B$$
$$\eta = \varphi_A + \varphi_B - \psi_c \quad (3)$$

with the critical composition obtained by setting the coefficient of the term of η^3 to zero

$$\psi_c = \frac{\sqrt{N_C}}{\sqrt{N_A}+\sqrt{N_C}}; \quad N_C = N_A + N_B \quad \text{and} \quad N_A = N_B \quad (4)$$

In the above equations, N_A, N_B, and N_C are the chain lengths of species A, B, and C. ψ_c is the critical composition of the phase diagram for the phase separation between C and A/B.

By expanding the Flory−Huggins free energy according to the order parameters η and ϕ defined in eq 2, we obtain

$$\begin{aligned} f(\eta,\phi) \approx & \left(\frac{\chi_{AB}}{4} - \frac{\chi_{AC}}{2} - \frac{\chi_{BC}}{2} + \frac{1}{4\psi_c N_A} + \frac{1}{4\psi_c N_B} + \frac{1}{2(1-\psi_c)N_C}\right)\eta^2 \\ & + \left(-\frac{1}{12\psi_c^2 N_A} - \frac{1}{12\psi_c^2 N_B} + \frac{1}{6(1-\psi_c)^2 N_C}\right)\eta^3 \\ & + \left(\frac{1}{24\psi_c^3 N_A} + \frac{1}{24\psi_c^3 N_B} + \frac{1}{12(1-\psi_c)^3 N_C}\right)\eta^4 \\ & + \left(-\frac{\chi_{AB}}{4} + \frac{1}{4\psi_c N_A} + \frac{1}{4\psi_c N_A}\right)\phi^2 + \left(-\frac{1}{12\psi_c^2 N_A} + \frac{1}{12\psi_c^2 N_B}\right)\phi^3 \\ & + \left(\frac{1}{24\psi_c^3 N_A} + \frac{1}{24\psi_c^3 N_B}\right)\phi^4 + \left(-\frac{\chi_{AC}}{2} + \frac{\chi_{BC}}{2} + \frac{1}{2\psi_c N_A} - \frac{1}{2\psi_c N_B}\right)\eta\phi \\ & + \left(-\frac{1}{4\psi_c^2 N_A} + \frac{1}{4\psi_c^2 N_B}\right)\eta^2\phi + \left(-\frac{1}{4\psi_c^2 N_A} - \frac{1}{4\psi_c^2 N_B}\right)\eta\phi^2 \\ & + \left(\frac{1}{4\psi_c^3 N_A} + \frac{1}{4\psi_c^3 N_B}\right)\eta^2\phi^2 + \left(\frac{1}{6\psi_c^3 N_A} - \frac{1}{6\psi_c^3 N_B}\right)\eta^3\phi \\ & + \left(\frac{1}{6\psi_c^3 N_A} - \frac{1}{6\psi_c^3 N_B}\right)\eta\phi^3 \end{aligned} \quad (5)$$

We assume that $N_C = 2N_A = 2N_B = 2N$, and the expansion can be simplified to

$$f_\eta(\eta) = -\frac{1}{2}c_1\eta^2 + \frac{1}{4}u_1\eta^4 \quad (6)$$

$$f_\phi(\phi) = -\frac{1}{2}c_2\phi^2 + \frac{1}{4}u_2\phi^4 \quad (7)$$

$$f_{int}(\eta,\phi) = b_1\eta\phi - \frac{b_2}{2}\eta\phi^2 + \frac{b_4}{2}\eta^2\phi^2 \quad (8)$$

with

$$c_1 = -\frac{\chi_{AB}}{2} + \chi_{AC} + \chi_{BC} - \frac{2+\sqrt{2}}{2\psi_c N}, \qquad u_1 = \frac{1}{3\psi_c^3 N(1-\psi_c)} \quad (9)$$

$$c_2 = \frac{\chi_{AB}}{2} - \frac{1}{\psi_c N}, \qquad u_2 = \frac{1}{3\psi_c^3 N} \quad (10)$$

$$b_1 = -\frac{\chi_{AC}}{2} + \frac{\chi_{BC}}{2} \quad (11)$$

$$b_2 = \frac{1}{\psi_c^2 N}, \qquad b_4 = \frac{1}{\psi_c^3 N} \quad (12)$$

The constant b_1 reflects the interaction comparison between species C with both A and B; in this work, we assume that the interaction parameters between C with A and B are the same i.e., $\chi_{AC} = \chi_{BC}$, then $b_1 = 0$. The interaction terms in eq 8 reflect

the competition of phase separation between C with A and B. Then, the model free energy for the ternary mixture in terms of η and ϕ is written as

$$F\{\eta,\phi\} = \int \mathrm{d}\mathbf{r}\,[f_\eta(\eta) + f_\phi(\phi) + f_{\mathrm{int}}(\eta,\phi)] + \frac{D_\eta}{2}\int \mathrm{d}\mathbf{r}(\nabla\eta(\mathbf{r}))^2 + \frac{D_\phi}{2}\int \mathrm{d}\mathbf{r}\,(\nabla\phi(\mathbf{r}))^2 \quad (13)$$

where D_η and D_ϕ are phenomenological parameters related to surface energy. For the sake of convenience, functions f_η, f_ϕ, and f_{int} are simplified as[19,20]

$$\frac{\mathrm{d}f_\eta}{\mathrm{d}\eta} = A_\eta \tanh\eta - \eta$$
$$\frac{\mathrm{d}f_\phi}{\mathrm{d}\phi} = A_\eta \tanh\phi - \phi \quad (14)$$

In the above equations, $A_\eta - 1 = c_1$ and $A_\phi - 1 = c_2$ are phenomenological parameters which are inversely proportional to temperature.

The kinetic equations describing the evolution of the order parameters of a ternary phase separating mixture coupled with reversible chemical reaction is written as a modified TDGL equation[10,11]

$$\frac{\partial\eta}{\partial t} = M_\eta\nabla^2\frac{\delta F\{\eta,\phi\}}{\delta\eta} + 2\Gamma_{-1}\varphi_{\mathrm{C}} - 2\Gamma_1\varphi_{\mathrm{A}}\varphi_{\mathrm{B}}$$
$$\frac{\partial\phi}{\partial t} = M_\phi\nabla^2\frac{\delta F\{\eta,\phi\}}{\delta\phi} \quad (15)$$

where M_η and M_ϕ are the mobility coefficients and F denotes the mixing free energy functional of the system. Using the above free energy functional F defined in eq 13, the CDS corresponding to the above TDGL equations is written as

$$\eta(\mathbf{r},t+1) = \eta(\mathbf{r},t) + \langle\langle J_\eta(\mathbf{r},t)\rangle\rangle - J_\eta(\mathbf{r},t) + 2(\Gamma_{-1}\varphi_{\mathrm{C}} - \Gamma_1\varphi_{\mathrm{A}}\varphi_{\mathrm{B}}) \quad (16)$$

$$\phi(\mathbf{r},t+1) = \phi(\mathbf{r},t) + \langle\langle J_\phi(\mathbf{r},t)\rangle\rangle - J_\phi(\mathbf{r},t) \quad (17)$$

$$J_\eta(\mathbf{r},t) = -D_\eta(\langle\langle\eta\rangle\rangle - \eta) - A_\eta\tanh\eta + \eta + b_1\phi - \frac{1}{2}b_2\phi^2 + b_4\eta\phi^2 \quad (18)$$

$$J_\phi(\mathbf{r},t) = -D_\phi(\langle\langle\phi\rangle\rangle - \phi) - A_\phi\tanh\phi + \phi + b_1\eta - b_2\eta\phi + b_4\eta^2\phi \quad (19)$$

The simulations of the model system are carried out in two-dimensional space with $L \times L = 256 \times 256$ square cells with periodic boundary conditions in both directions. In CDS, $\langle\langle \mathrm{X}\rangle\rangle$ is defined as the sum of the nearest neighbors (NN) of X and the next nearest neighbors (NNN) of X

$$\langle\langle \mathrm{X}\rangle\rangle = \frac{1}{6}\sum_{\mathrm{NN}}\mathrm{X} + \frac{1}{12}\sum_{\mathrm{NNN}}\mathrm{X} \quad (20)$$

In the cell dynamic simulations, we set $M_\eta = M_\phi = 1.0$, $D_\eta = D_\phi = 0.5$, $\psi_{\mathrm{C}} = 0.586$, $b_1 = 0$, $b_2 = 0.3$, and $b_4 = 0.3/\psi_{\mathrm{C}}$. In present simulation work, in the case of $A_\phi = 1.3$ and $A_\eta = 1.1$, from eq 9 to eq 12, it can be obtained that $\chi_{\mathrm{AB}} \simeq 0.95$, $\chi_{\mathrm{BC}} = \chi_{\mathrm{AC}} \simeq 0.44$, $\chi_{\mathrm{AB}}N \simeq 9.5$, and $\chi_{\mathrm{BC}}N = \chi_{\mathrm{AC}}N \simeq 4.4$. In the case of $A_\phi = 1.1$ and $A_\eta = 1.3$, $\chi_{\mathrm{AB}} \simeq 0.55$, $\chi_{\mathrm{BC}} = \chi_{\mathrm{AC}} \simeq 0.44$, $\chi_{\mathrm{AB}}N \simeq 5.5$, and $\chi_{\mathrm{BC}}N = \chi_{\mathrm{AC}}N \simeq 4.4$.

We should mention that for the given kinetic rate constants of $\Gamma_1 = \Gamma_{-1} = \Gamma$ in the homogeneous state, the equilibrated concentrations of A, B and C can be calculated according to the following equation

$$\frac{\Gamma_{-1}}{\Gamma_1} = 1.0 = \frac{\langle\varphi_{\mathrm{A}}\rangle_{\mathrm{e}}\langle\varphi_{\mathrm{B}}\rangle_{\mathrm{e}}}{\langle\varphi_{\mathrm{C}}\rangle_{\mathrm{e}}} = \frac{\langle\varphi_{\mathrm{A}}\rangle_{\mathrm{e}}\langle\varphi_{\mathrm{B}}\rangle_{\mathrm{e}}}{1 - \langle\varphi_{\mathrm{A}}\rangle_{\mathrm{e}} - \langle\varphi_{\mathrm{B}}\rangle_{\mathrm{e}}} \quad (21)$$

and we obtain that $\langle\varphi_{\mathrm{A}}\rangle_{\mathrm{e}} = \langle\varphi_{\mathrm{B}}\rangle_{\mathrm{e}} \approx 0.4142$ and $\langle\varphi_{\mathrm{C}}\rangle_{\mathrm{e}} \approx 0.1716$. In this simulation, we set the averaged initial local volume fractions of the ternary mixture as $\langle\varphi_{\mathrm{A}}\rangle = \langle\varphi_{\mathrm{B}}\rangle = 0.3$ and $\langle\varphi_{\mathrm{C}}\rangle = 0.4$, and the system is assumed to be homogeneous. Therefore, the system is quite close to the equilibrium state of the homogeneous system. However, we will see in the next section that this chemical equilibrium state for homogeneous system can never be reached due to the phase separation. The system is then quenched to unstable phase region to initiate phase separation of the ternary mixture. Because of the change of the local concentrations of species, chemical reaction simultaneously takes place in order to establish new equilibrium. For simplicity, the forward and backward reaction rate constants are set equal, and they are the same before and after the temperature quenching.

III. Simulation Results and Discussions

III.1. $A_\eta = 1.1$ and $A_\phi = 1.3$. In this case, the compatibility between A and B is quite poor, and thus, the driving force for the phase decomposition between the species A and B is strong, while the component C has relatively good compatibility with both A and B. The evolution of domain patterns with the chemical reaction rate constant $\Gamma = 0.001$ are shown in Figure 1. It is seen from Figure 1 that when $\tau = 500$, the phase separation between A and B takes place due to the poor compatibility between A and B, which forms the bicontinuous phase composed of A-rich and B-rich domains. The species C is then pushed to the interface between A-rich and B-rich domains. As the driving force for the phase separation between A and B is quite strong, in the A-rich and B-rich domains, there are almost pure A and B, and thus, the chemical reaction can almost only happen at the interface of phase domains. Therefore, it can be expected that the patterns formed are similar to that formed by phase separation of the binary mixture with the addition of surfactant molecules.[21,22,23] Kawakatsu and Kawasaki[24,25,26,27] have described the discrete surfactant molecules using hybrid model with microspin vector and concentration scalar, and the simulation results revealed that most of the surfactant molecules segregate on the interface of the phase domains. Komura[28] et al. treated the surfactants as the third ingredient, avoiding the computational complexity due to vector operation. By using two TDGL equations to simulate water−oil system with the addition of surfactant molecules, the similar phase patterns are obtained. The corresponding experimental analogue is the binary mixture of homopolymers A and B with the addition of small amount of block copolymer A−B, which improves the compatibility of A and B. In the blends of homopolymers A and B, the block copolymer segregate onto the interface between A-rich and B-rich domains, emulsifying the system.[29,30] As the phase separation between A and B proceeds ($\tau = 1000$), the domain sizes of the A- and B-rich phases gradually increase, while the concentration of species C

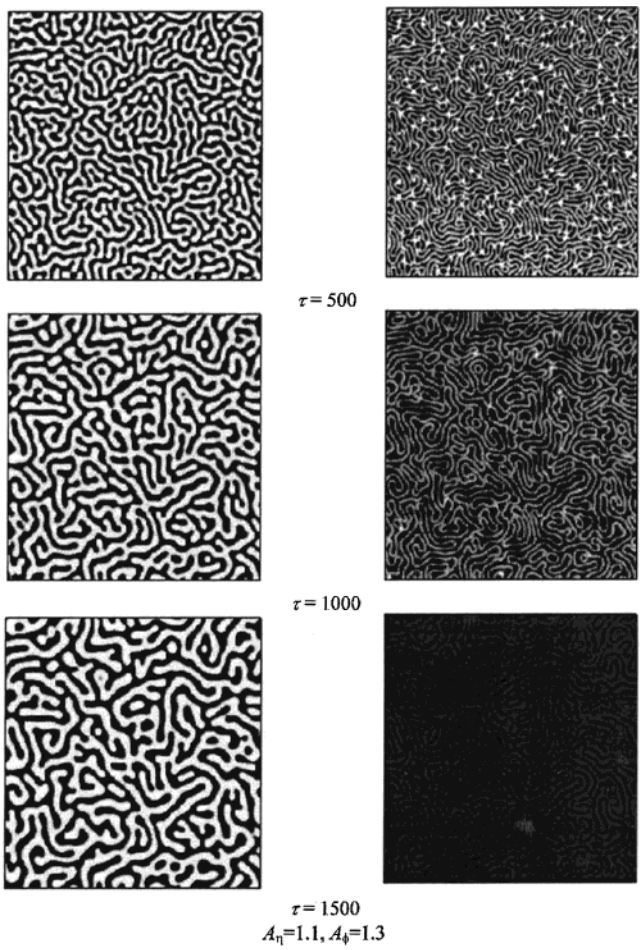

Figure 1. Time evolution of domain patterns. The model parameters are $M_\eta = M_\phi = 1$, $D_\eta = D_\phi = 0.5$, $\psi_c = 0.586$, $A_\eta = 1.1$, $A_\phi = 1.3$, and $\Gamma = 0.001$. The interaction parameters are $b_2 = 0.3$ and $b_4 = 0.3/\psi_c$. The average concentration of A, B, and C are $\langle\varphi_A\rangle = \langle\varphi_B\rangle = 0.3$ and $\langle\varphi_C\rangle = 0.4$. The left column displays the spatial distribution of the ϕ field, in which white regions correspond to positive ϕ (or φ_A) and black regions correspond to negative ϕ (or φ_B). The right column shows the spatial distribution of φ_C, in which white regions correspond to large φ_C.

decreases drastically from the initial value of $\langle\varphi_C\rangle = 0.4$, due to the decomposition of C in the C-rich domains. The decomposition of C increases the concentrations of A and B continuously until the local equilibrium has been reached. However, due to the proceeding of phase separation of A and B, the product of the local concentrations $\varphi_A\varphi_B$ in both A- and B-rich phases decreases gradually. Therefore, the forward chemical reaction is inhibited, and the equilibrium is dictated by the backward reaction. As the evolution of phase separation further proceeds, the growth of domains continues, and the local concentration of C at the interfaces between A- and B-rich domains decreases to an extremely low level. To our surprise, the local concentration of C at the interface is even lower than that in either A- or B-rich domains ($\tau = 1500$). We attribute this phenomenon to the mutual competition between phase separation and chemical reaction. The outcome of these mutual competitions is that the phase separation of A and B enriches C to the domain interface. During the enrichment of C at the domain interface, the decomposition of C at the interface accelerates.

Obviously, when the reaction rate constant is very small ($\Gamma = 0.00001$), the chemical reaction proceeds very slowly, and

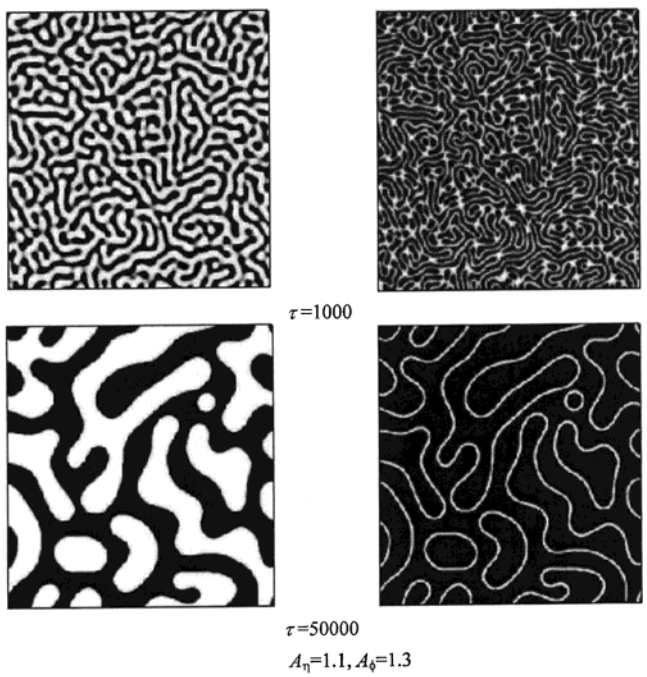

Figure 2. Time evolution of domain patterns. All the parameters are the same as those in Figure 1 except $\Gamma = 0.00001$.

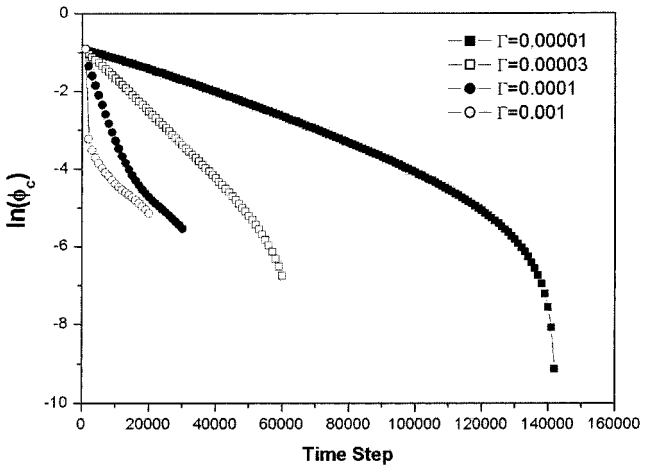

Figure 3. Evolution of the concentration of C in the case of various Γ in the $\ln\langle\phi_c\rangle - t$ scale. All other parameters are the same as those in Figure 1.

the phase separation patterns resemble those of ternary mixtures. It can be seen from Figure 2 that, different from that in Figure 1, at the late stage of evolution, species C still segregates on the interface between A-rich domains and B-rich domains ($\tau =$ 50 000). As the reaction rate constant decreases gradually (from $\Gamma = 0.001$ to $\Gamma = 0.00001$), the competition due to chemical reaction decays. The evolutions of the total concentration of C for various Γ are shown in Figure 3 in $\ln\langle\varphi_c\rangle - t$ scale. It is seen from Figure 3 that the concentration of C decay exponentially before it reaches diminishingly small value. The decay exponent is proportional to the slope of the line. From the slopes at various reaction rate constant Γ, we find that the decay exponent is proportional to the reaction rate constant Γ. For $\Gamma = 0.0001$, the domain pattern at $\tau = 50\,000$ is just a snapshot of an intermediate state. In essence, the global picture of phase separation of the ternary mixture at steady state is the phase separation of binary mixture of A and B, while species C

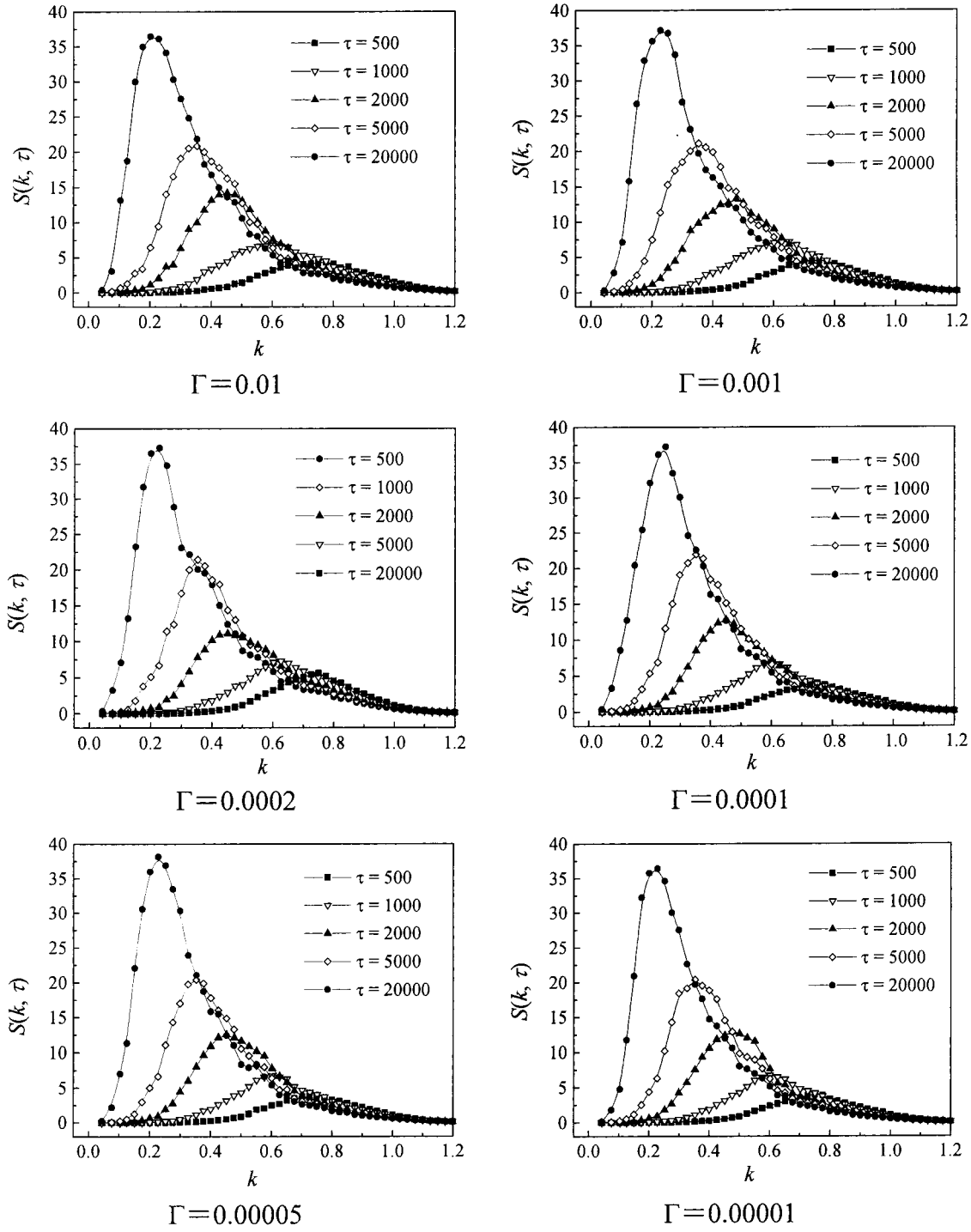

Figure 4. Spherical averaged structure factors $S(k,\tau)$ in the case of various Γ. All other parameters are the same as those in Figure 1.

completely transformed to A and B. Therefore, the global equilibrium which exists in the homogeneous system calculated in eq 21 does not exist any more. However, we should mention in advance that this is not always the case. When the compatibility between C and A/B is much poor than that between A and B ($A_\eta = 1.3$ and $A_\phi = 1.1$), the overall concentration of C is increasing as decreasing the chemical reaction rate constant. The overall concentration of C can be even higher than the equilibrium concentration in the homogeneous system. The detailed discussion can be found in the following subsections, and the results are shown in Figures 9 and 10.

To quantitatively characterize the domain evolution for the system at $A_\eta = 1.1$ and $A_\phi = 1.3$, we concentrated our attention on the evolution of A-rich and B-rich domains, which can be evaluated by the structure factor $S_k(\tau) = \langle \phi_k \phi_{-k} \rangle$ with ϕ_k the Fourier transformation of $\phi(\mathbf{r})$. Figure 4 shows the time evolution profile of the spherically averaged structure factor at various chemical reaction rate constants. The peak in each structure factor curve reflects the domain sizes. The peak intensities increase, and the peaks shift to lower k values as the phase separation proceeds, and the profiles in the right side of the peaks form an envelope, which resembles the phase separation dynamics of polymer blends with asymmetrical molecular weights.[31] The growth of domain can be evaluated by the time evolution of peak position $k_m(\tau)$. Because of the difficulty of defining the peak positions precisely, we resort to

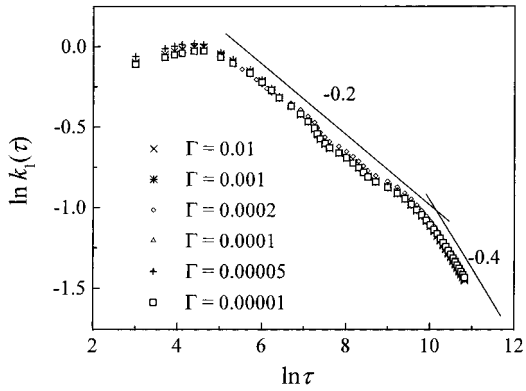

Figure 5. Time evolution of the first moment of the structure factor, $k_1(\tau)$, according to the spherical averaged structure factors $S(k,\tau)$ in Figure 4. The evolution curves show three stages: early stage, intermediate stage, and late stage. Nearly all the curves with different Γ are overlapped.

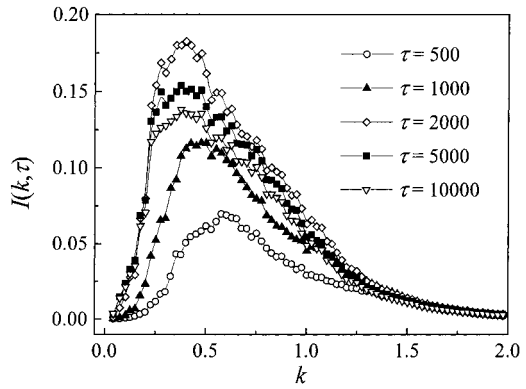

Figure 6. Spherical averaged structure factors $I(k,\tau)$ with Γ = 0.0001. All other parameters are the same as those in Figure 1.

the first moment $k_1(\tau)$ of the structure factor to characterize the domain sizes, which is defined as

$$k_1(\tau) = \frac{\sum_k kS(k,\tau)}{\sum_k S(k,\tau)} \tag{22}$$

The scaling laws of $k_1(\tau)$ and $k_m(\tau)$ are the same in the growth exponent.[32] Experimental and simulation results confirm that in the late stage of phase separation, $k_1(\tau)$ (or $k_m(\tau)$) obey the following scaling law:

$$k_1(\tau) \propto \tau^{-\alpha} \tag{23}$$

where α is Lifshitz−Slyozov growth exponent.[33] Neglecting the hydrodynamic effects and the viscoelastic effect, α should be $^1/_3$. To our surprise, in our simulation, all ln $k_1(\tau) \sim \ln \tau$ curves superimposed with each other, irrelevant to the change of Γ (Figure 5). Figure 5 also reveals that the growth of domains can be divided into three stages: early stage, middle stage, and late stage. The growth exponent in the middle stage is 0.2, while the growth exponent in the late stage is 0.4. In the middle stage of phase separation, the segregation of species C at the interface of A- and B-rich domains inhibits the domain growth, which resembles the inhibition of domain growth in the binary polymer blends with the addition of surfactant or block copolymer molecules.[29,30] In the late stage of phase separation, due to the drastic decrease of the concentration of species C, the effect of

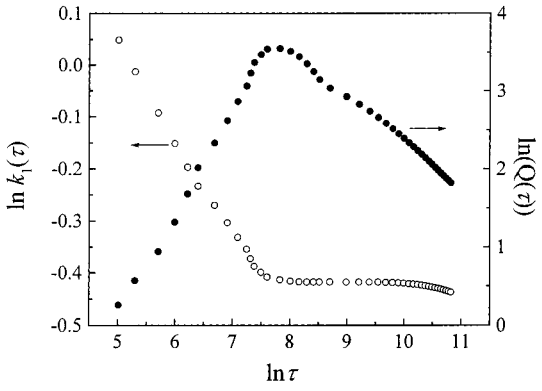

Figure 7. Time evolution of the first moment of the structure factor, k_1, and the global order parameter Q according to the spherical averaged structure factors $I(k,\tau)$ in Figure 6, with Γ = 0.0001.

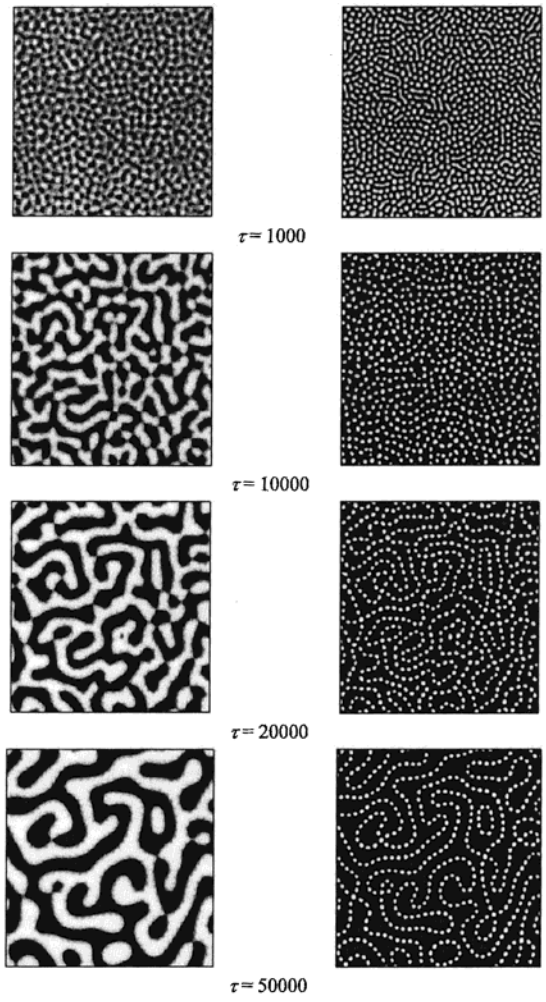

Figure 8. The time evolution of domain patterns. All the parameters are the same as those in 1 except $A_\eta = 1.3$, $A_\phi = 1.1$, and Γ = 0.01. The left column displays the spatial distribution of the ϕ field, and the right column shows the spatial distribution of φ_C.

species C as interface compatibilizer diminishes. On the contrary, the chemical reaction accelerates the domain growth. Looking carefully at the domain growth during the middle stage of phase separation shown in Figure 5, we observed a small inflection of domain growth at $\tau \approx 1600$. This inflection in domain growth must be closely related to the chemical reaction and the distribution of order parameter η. To confirm it, we have calculated the evolution profile of spherically averaged structure factor $I_k(\tau) = \langle \eta_k \eta_k \rangle$ (cf. Figure 6) for the case of Γ =

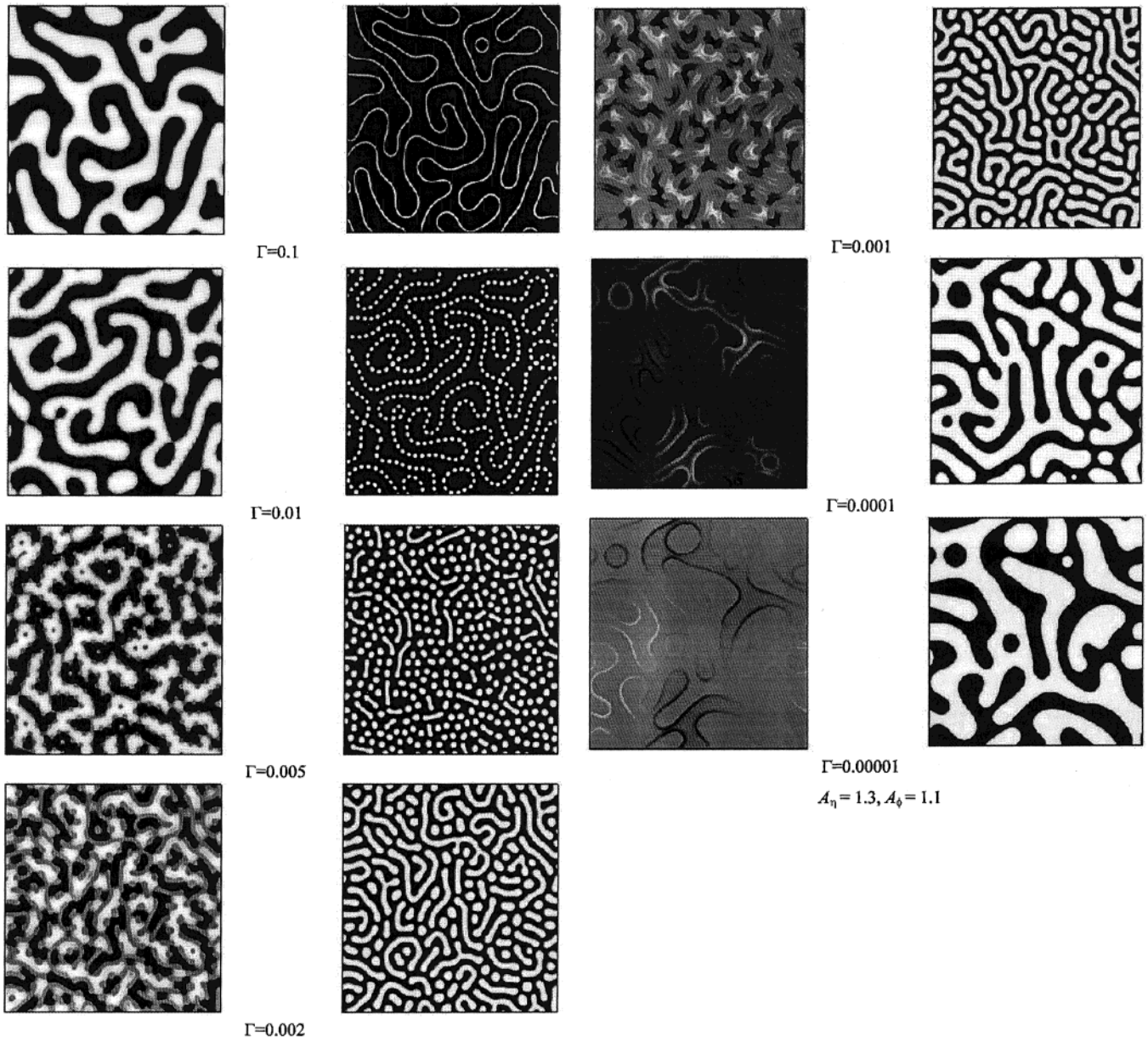

Figure 9. Domain patterns at $\tau = 50000$ with various Γ values. All other parameters are the same as those in Figure 8. The left column displays the spatial distribution of the ϕ field, and the right column shows the spatial distribution of φ_C.

0.0001, following the same procedure as that for $S_k(\tau)$. As the phase separation proceeds in the early-middle stages, the peaks in the profiles of the structure factors shift to the direction of lower k, and the peak intensities gradually increase. However, after the evolution passes a certain critical threshold, the peak intensities gradually decrease while keeping the peak position unchanged. It can be imagined that the peak intensities of the structure factor profile increase as the phase separation evolves in the early-middle stages and then decrease due to the decomposition chemical reaction of species C in the late and middle stages. The time evolution of the first moment $k_1(\tau)$ of the structure factor $I_k(\tau)$ is shown in Figure 7, which indicates that, at early stage, the domain size increases exponentially and then keeps at constant level as evolution passes $\tau \approx 1600$. To compare the peak heights quantitatively, we introduce a global order parameter Q that is defined as

$$Q = \sum_k kI(k) \tag{24}$$

Q corresponds to the total scattering light intensity in experiment. It can be seen from Figure 7 that the peak position of the Q evolution is located at $\tau \approx 1600$, where the effects of phase separation and chemical reaction upon the evolution of order parameter η are comparable with each other. Before this time, the effect of phase separation dominates, while the effect of chemical reaction takes over after this turning point. It is exactly the change of the behavior of order parameter η at $\tau \approx 1600$ which triggers the inflection in the curve of domain growth at this particular time. However, the reaction rate constant Γ has little influence upon this turning point in time evolution.

III.2. $A_\eta = 1.3$ and $A_\phi = 1.1$. In this case, the species A and B are mutually compatible, while the reaction product C has relatively poor compatibility with both A and B. The evolution of domain patterns at $\Gamma = 0.01$ is shown in Figure 8. It is seen form Figure 8 that at the early stage of phase evolution ($\tau \approx 1000$), the relatively good compatibility renders A and B agglomerating together and thus A/B phase separate with C. The morphologies shown in Figure 8 reveal that the phase separation between C and A/B takes place via the mechanism of nucleation and growth; i.e., the nucleated C-rich droplets are

dispersed in the continuous domain of A and B. As phase patterns further evolve (τ = 10 000 and 20 000), the phase separation between A and B starts, and thus, it pushes the C-rich droplets to the interface between A- and B-rich domains. As discussed in the previous subsection, due to the phase separation between A and B, C in the C-rich droplets will gradually decompose to A and B. Therefore, the size and the total volume fraction of C-rich droplets decrease accordingly. In the late stage of phase evolution (τ = 50 000), the C-rich droplets distribute along the interface between A- and B-rich domains completely, forming the necklace-like patterns of C-rich droplets.

We have mentioned in advance in the last subsection that the phase morphology and the overall concentration of C depend on the chemical reaction rate constant strongly. The effect of chemical reaction rate constant on the phase pattern is illustrated in Figure 9. It is seen from Figure 9 that the rate of chemical reaction dramatically affects the evolution of phase patterns. To understand the phase patterns generated from the systems with different chemical rate constants, we have to carefully consider the details of the process. We imagine that in the initial stage, C-rich droplets are formed and distributed throughout the continuous phase of A and B due to the poor compatibility between C and A/B. However, due to the chemical reaction involved, C in C-rich domains will decompose to A and B. Because of the same reason, A and B in the A- and B-rich phases will convert to C. In essence, the chemical reaction homogenizes the system and competes with the phase separation process. In the case of high reaction rate constant $\Gamma = 0.1$, the effect of chemical reaction is dominant; once the C-rich domain is formed, it decomposed into A and B almost immediately. Then the phase separation between the components A and B proceeds and forms the A- and B-rich domains. The forward chemical reaction is then prohibited due to the phase separation between A and B. Therefore, as the phase separation between A and B proceeds, C continuously decomposes to A and B, and the residual small amount of C segregate along the interface between A-rich and B-rich domains. It resembles the case of $A_\eta = 1.1$ and $A_\phi = 1.3$ with $\Gamma = 0.00001$ shown in Figure 2 discussed previously. As the reaction rate constant decreases, the effect of chemical reaction upon the evolution of phase patterns diminishes, and the driving force of phase separation begins to take over. The phase patterns are more or less like the phase separation of ternary mixture absent of chemical reactions. It is really important to note that due to the absence of the global equilibrium existed in homogeneous system, the concentration of species C at very late stage increases as the reaction rate constant decreases, as shown in Figure 10, and the morphological pattern of C changes from dispersed phase to continuous phase. It is also interesting to note that the phase separation between A and B is confined in small regions (cases of $\Gamma = 0.001$ and 0.002), forming microphase separation patterns similar to those of block copolymers. It can also be seen in Figure 10 that in the initial stage of phase evolution and the intermediate chemical reaction rate constants, the concentration of C decreases first and then begins to increase. Eventually, it turns to decrease to the steady values. This unusual feature reflects the competition between the evolutions of order parameters ϕ and η, which describe the phase separations between C and A/B and between A and B. Figure 11 shows the evolution profile of the first moments of structure factors, $k_1(\phi,\tau)$ and $k_1(\eta,\tau)$, with the chemical reaction rate constant $\Gamma = 0.01$. By comparing to Figure 8, it is seen from Figure 11 that the phase separation between C and A/B takes place at $\tau \approx 150$. However, the phase separation between A and B starts later at $\tau \approx 600$.[34]

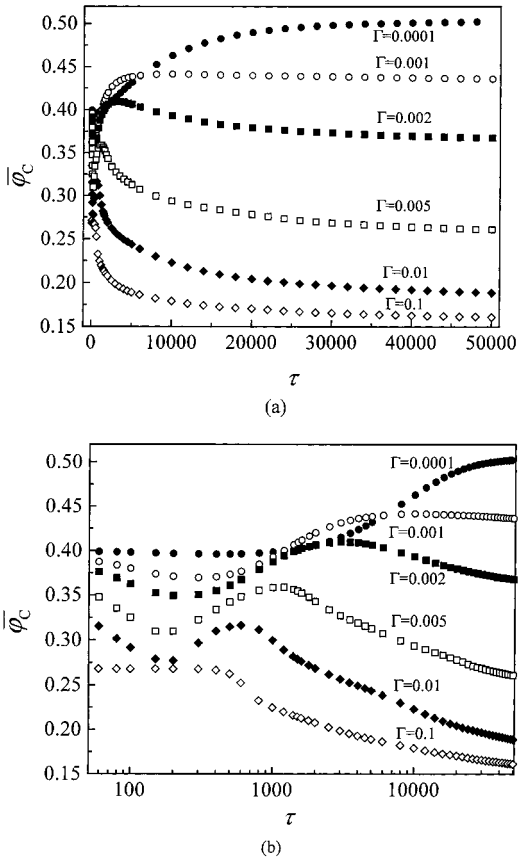

Figure 10. Evolution of the concentration of C in the case of various Γ. All other parameters are the same as those in Figure 8. The evolution curves show that the average concentration of C increases when Γ decreases at late stage of phase separation. In the early evolution time, the average concentration of C decreases first and then increases. To discern this variety easily, the curves are also plotted with logarithm coordinate (b).

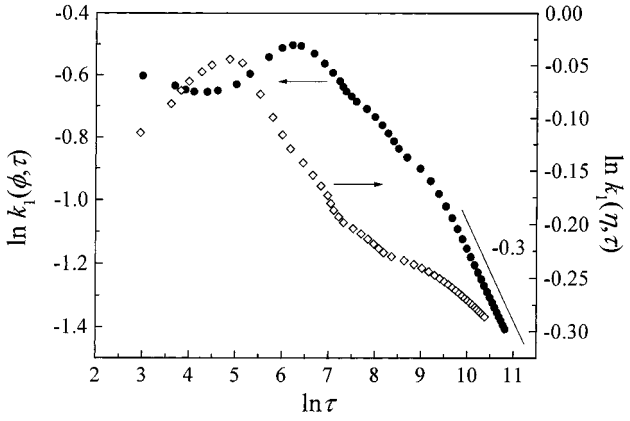

Figure 11. Time evolution of the first moment of the structure factor$S(k,\tau)$ and $I(k,\tau)$, according to the pattern formations in Figure 8 with $\Gamma = 0.01$.

At the initial stage of phase separation ($\tau < 150$), the system is homogeneous and meanwhile C decomposes to A and B. When $\tau > 150$, due to the phase separation between C and A/B, the concentration of C slightly increases. When $\tau > 600$, the phase separation between A and B drives the chemical reaction backward and reduces the concentration of C slightly. The characteristic time at which the fluctuation of the concentration of C happens corresponds to the time at which the evolution of order parameters η and ϕ transits from the initial stage to the middle stage of phase separation. Figure 11 has also indicated

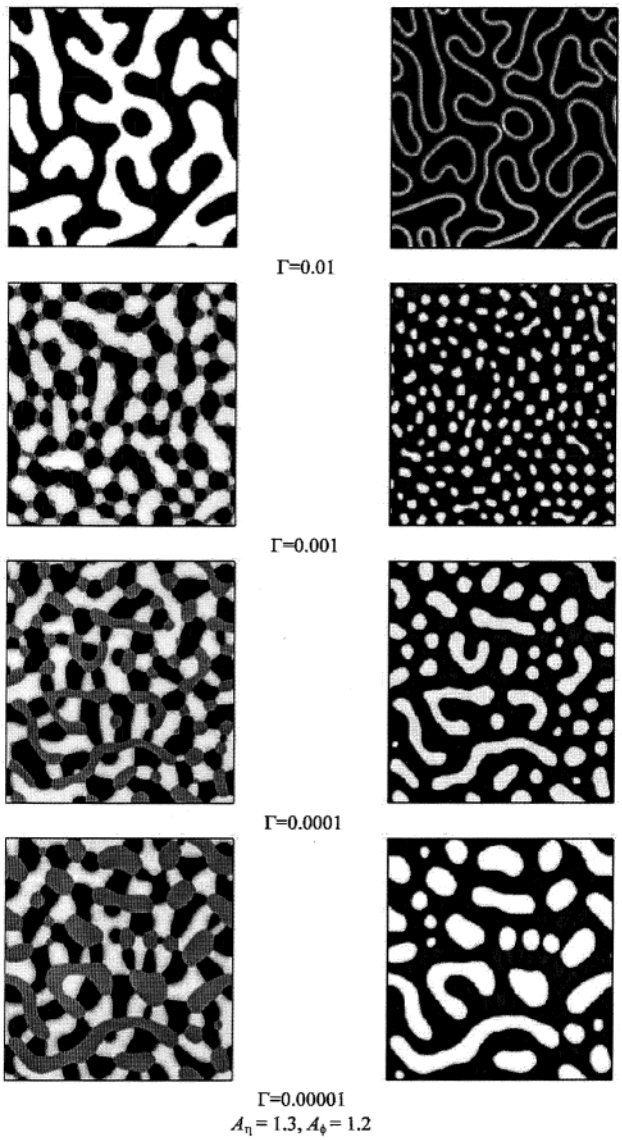

Figure 12. Domain patterns at $\tau = 50000$ with various Γ. All other parameters are the same as those in Figure 10 except $A_\eta = 1.3$ and $A_\phi = 1.2$. The left column displays the spatial distribution of the ϕ field, and the right column shows the spatial distribution of φ_C.

that in the late stage, the domain growth of phases A and B follows the Lifshitz−Slyozov scaling law with $\alpha \approx 1/3$.

III.3. $A_\eta = 1.3$ and $A_\phi = 1.2$. Here we consider the case of $A_\eta = 1.3$ and $A_\phi = 1.2$. In this case, the compatibility between A and B is between the cases discussed in the last two subsections. Therefore, the phase separation between A and B plays a more important role in the evolution of phase patterns than the case discussed in the last subsection. Figure 12 shows the phase patterns at various Γ in the late stage of phase separation ($\tau = 50\,000$). It is seen from Figure 12 that when Γ is relatively large (Γ = 0.01), the phase separated C rapidly decomposes into A and B as the phase separation between A and B proceeds. Meanwhile, the residual C segregates on the interface between A- and B-rich domains. When Γ = 0.001, the decomposition of C slows down and the phase separated C forms dispersed droplets immersed in A/B matrix. Meanwhile, due to the incompatibility between A and B, the phase decomposition between A and B then takes place in the confined regions where originally the continuos domain of A/B exists. This characteristic domain morphology can be more clearly seen when Γ is even lower, i.e., Γ = 0.0001 and 0.00001.

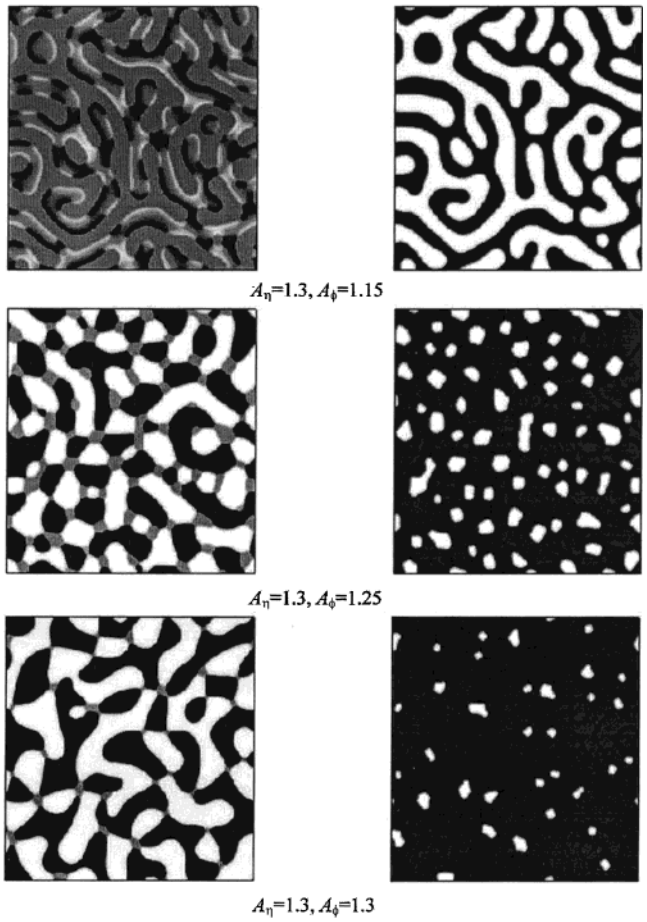

Figure 13. Domain patterns at $\tau = 50\,000$ with Γ = 0.0001. All other parameters are the same as those in Figure 9 except A_η and A_ϕ. The left column displays the spatial distribution of the ϕ field, and the right column shows the spatial distribution of φ_C.

III.4. Effect of the Interaction Parameters A_η and A_ϕ. It is seen from the discussion given above that even for the ternary mixture coupled with such a simple chemical reaction, the spatial-temporal behaviors of the system is quite complex. The kinetics and phase patterns of this system are dependent on at least the following factors, such as the initial composition, the rate constants of the chemical reaction, and the interaction parameters A_η and A_ϕ, etc. To investigate the effect of compatibility between the components on morphology, here we briefly investigate the effect of interaction parameters on the morphology.

In the following discussion, we fix $A_\eta = 1.3$ and Γ = 0.0001 while varying A_ϕ from 1.15 to 1.3 to study the morphologies of the late stage ($\tau = 50\,000$, Figure 13). In these cases, C and A/B are extremely incompatible, and the driving force for the phase separation between A and B is strengthened gradually. When $A_\phi = 1.15$, C is incompatible with A/B, and thus, the phase separation between C and A/B proceeds more thoroughly, while the phase separation between A and B proceeds only slightly. The chemical reaction of forming C mainly takes place in the phase of A/B and then diffuses into the C-rich phase. Thus, the volume fraction of C in this case is increased. When A_ϕ is increased to 1.25, the species A and B segregate more strongly, and thus, the chemical reaction between A and B can only happen at the interface between A- and B-rich domains. Therefore, it results in the strong reduction of the volume fraction of C. As A_ϕ is further increased to 1.3, A and B decompose more strongly, and thus, the volume fraction of C at the late stage is further reduced.

IV. Conclusions

In this paper, we have numerically investigated the phase evolution of an A, B and C ternary mixture coupled with the chemical reaction of $A + B \underset{\Gamma_{-1}}{\overset{\Gamma_1}{\rightleftarrows}} C$. The numerical simulation is carried on a two-dimensional square lattice based on the modified TDGL equation. It is found that when the system is quenched from homogeneous phase region to unstable phase region, the phase separation and chemical reaction come into play simultaneously. Through the above numerical simulation, the following conclusions can be drawn:

(1) If the compatibility of A and B is relatively poor while C has relatively good compatibility with A/B, in the early stage of phase evolution, the phase separation between A and B pushes C to the interface between A- and B-rich domains. The domain growth continues as time evolution proceeds, and the concentration of C decreases drastically. As the evolution proceeds to the late stage, the concentration of C at the interface is even lower than that in A-rich and B-rich phases. At steady state, the global picture is the phase separation of binary mixture of A and B, which form bicontinuous phase pattern, while species C decomposes completely to A and B.

(2) If A and B are compatible with each other while C and A/B are incompatible, in the early stage of phase evolution, C-rich spherical droplets are immersed in the A/B continuous phase. As evolution goes on, the phase separation of A and B takes place, and pushes C droplets to the interface between A- and B-rich domains. The phase evolution depends on the competition between chemical reaction and phase separation. In the case of relatively large reaction rate constant, the effect of chemical reaction is dominant, the phase separation between C and A/B is inhibited, and the phase separation between A and B takes place. As the phase separation of A and B proceeds, C decomposes into A and B rapidly, resulting in the phase pattern of small amount of C distributed on the interface between A- and B-rich domains. As the reaction rate constant gradually decreases, the effect of chemical reaction is diminishing. In the late stage of phase separation, the steady-state concentration of C increases as the rate constant of chemical reaction decreases, and the C-rich phase changes from dispersed droplets to the continuous thin phase. Then the phase separation between A and B is confined in small regions, resembling the case of binary mixture of A and B homopolymers with AB diblock copolymers. The domain growth of A and B follows the Lifshitz-Slyozov scaling law with $\alpha \approx {}^1/_3$ in the late stage of phase evolution.

(3) Due to the phase separation between the components A, B, and C, the global equilibrium, which exists in the homogeneous mixture, does not exist in the phase separating system. The overall volume fraction of C could be either lower or higher than the equilibrium value for the homogeneous mixture, depending on the compatibility between the components and the rate constant of coupled chemical reaction.

Finally, we should mention that the phase separating mixture coupled with chemical reaction is quite complex. One could imagine that the system will become more and more complex when the chemical reaction has higher complexity, especially for the nonlinear or auto-catalytic reaction, which deserves further theoretical and experimental studies.

Acknowledgment. This work is subsidized by the State Key Project on the Basic Research of China, NSF of China and the Special Funds for Major State Basic Research Projects (G1999064800). We would also like to thank Dr. Z.-G. Wang from CALTEC, Pasadena, CA, USA, for helpful discussions and suggestions.

References and Notes

(1) For example, see: Manneville, P. *Dissipative Structures and Weak Turbulence*; Academic Press: New York, 1990.
(2) Dee, G. T.; Langer, J. S. *Phys. Rev. Lett.* **1986**, *50*, 383.
(3) Barelko, V. V. Self-organization Phenomena and Autowave Processes in Heterogeneous Chemical and Physical Systems. In *Self-organization, Autowaves and Structures Far from Equilibrium*; Krinsky, V. I., Ed.; Springer-Verlag: Berlin, 1984; p 164.
(4) Cross, M. C.; Hohenberg, P. C. *Rev. Mod. Phys.* **1993**, *65*, 851.
(5) Cahn, J. W. *Acta Metall.* **1961**, *9*, 795.
(6) Binder, K. In *Material Science and Technology*: *Phase Transformations in Materials*, Vol. 5; Haasen, P., Ed.; VCH: Weinheim, Germany, 1990; p 405.
(7) Zhang, J.; Zhang, H.; Yang, Y. *Sinica China* **1996**, *B26*, 1496.
(8) Kataoka, K.; Urakawa, O.; Nishioka, H.; Tran-Cong, Q. *Macromolecules* **1998**, *31*, 8809.
(9) Tran-Cong, Q.; Harada, A. *Phys. Rev. Lett.* **1996**, *76*, 1162.
(10) Glotzer, S. C.; Stauffer, D.; Jan, N. *Phys. Rev. Lett.* **1994**, *72*, 4109.
(11) Glotzer, S. C.; Di Marzio, E. A.; Muthukumar, M. *Phys. Rev. Lett.* **1995**, *74*, 2034.
(12) Van Kampen, N. G. *Stochastic Process in Physics and Chemistry*; North-Holland: Amsterdam, 1992.
(13) Coleman, M. M.; Graf, J. F.; Painter, P. C. *Specific Interaction and the Miscibility of Polymer Blends*; Technomic Publishing Co.: Lancaster, PA, 1991.
(14) Smith, P.; Hara, M.; Eisenberg, A. *Current Topics in Polymer Science*; Ottenbrite, R., Utracki, L., Inoue, T., Eds.; Hanser Press: New York, 1987; Vol. 2.
(15) Oono, Y.; Puri, S. *Phys. Rev. Lett.* **1987**, *58*, 836; *Phys. Rev. A* **1994**, *38*, 434.
(16) Oono, Y.; Shiwa, Y. *Mod. Phys. Lett.* **1987**, *B1*, 49.
(17) He, D. Q.; Kwak, S.; Nauman, E. B. *Macromol. Theory Simul.* **1996**, *5*, 801.
(18) Huang, C.; Olvera de la Cruz, M.; Swift, B. W. *Macromolecules* **1995**, *28*, 7996.
(19) Ito, A. *Phys. Rev. E* **1998**, *58*, 6158.
(20) Ohta, T.; Ito, A. *Phys. Rev. E* **1995**, *52*, 5250.
(21) Laradji, M.; Guo, H.; Grant, M.; Zuckermann, M. J. *J. Phys. A: Math. Gen.* **1991**, *24*, 628.
(22) Laradji, M.; Guo, H.; Grant, M.; Zuckermann, M. J. *J. Phys.: Condens. Matter* **1992**, *4*, 6715.
(23) Kim, S. H.; Jo, W. H.; Kim, J. *Macromolecules* **1996**, *29*, 6933.
(24) Kawakatsu, T.; Kawasaki, K. *Phys. A* **1991**, *167*, 690.
(25) Kawakatsu, T.; Kawasaki, K. *J. Colloid Interface Sci.* **1991**, *145*, 413; **1991**, *145*, 420.
(26) Kawakatsu, T.; Kawasaki, K.; Furusaka, M.; Okabayashi, H.; Kanaya, T. *J. Chem. Phys.* **1993**, *99*, 8200.
(27) Kawakatsu, T.; Kawasaki, K.; Furusaka, M.; Okabayashi, H.; Kanaya, T. *J. Phys.: Condens. Matter* **1994**, *6*, 6385.
(28) Komura, S.; Kodama, H. *Phys. Rev. E* **1997**, *55*, 1722.
(29) Roe, R. J.; Kuo, C. M. *Macromolecules* **1990**, *23*, 4635.
(30) Hashimoto, T.; Izumitani, T. *Macromolecules* **1993**, *26*, 3631.
(31) Zhang, H.; Zhang, J.; Yang, Y. *Macromol. Theory Siml.* **1995**, *4*, 811.
(32) Glotzer, S. C.; Gyure, M. F.; Sciortino, F.; Coniglio, A.; Stanley, H. E. *Phys. Rev. E* **1994**, *49*, 247 and references therein.
(33) Lifshitz, I. M.; Slyozov, V. V. *J. Chem. Phys. Solids* **1961**, *19*, 35.
(34) The time of phase separation discussed here donates the time where the phase separation proceeds from the early stage to middle stage of phase evolution.